Modeling Reverse Osmosis Separations with Strong Solute-Membrane Affinity at Different Temperatures Using the Finely Porous Model

P. J. CONNELL* and J. M. DICKSON,† *Department of Chemical Engineering, McMaster University, Hamilton, Ontario, Canada, L8S 4L7*

Synopsis

The reverse osmosis separation of toluene from water has been studied using an asymmetric cellulose acetate membrane at different temperatures, pressures, and feed concentrations. The finely porous transport model is used to describe the performance of the membrane as a function of the operating conditions. Based on experimental data, the transport parameters for the membrane are estimated. These parameters include the pore size of the membrane, the frictional parameter for the solute in the membrane pore, the relative porosity of the membrane surface, and the partition coefficients on the high and low pressure sides of the membrane. The influence of operating temperature on some of these parameters is presented and discussed. A modified form of the finely porous model which includes the effect of temperature is presented.

INTRODUCTION

Although much effort has been spent in the development of mathematical models to describe mass transport in reverse osmosis (RO) membranes, the subject still remains controversial. Many models have been developed over the years; each being individual in premise and assumptions. Most of the models illustrate good agreement for inorganic solute systems, and many organic systems. However, for reverse osmosis systems involving strong solute–membrane affinity, most of the models perform poorly. The reason for this modelling limitation is due to the strong influence that solute–membrane affinity has on reverse osmosis transport phenomena.[1-6] One model that has been successful at describing reverse osmosis performance in the presence of strong solute–membrane affinity is the finely porous model (FPM). The qualitative differences between the case when solvent–membrane affinity dominates and when solute–membrane affinity dominates are summarized as follows:[7]

When solvent–membrane affinity dominates:

1. Increasing the operating pressure usually increases separation.
2. The decrease in permeate flux with increasing feed concentration is due to osmotic pressure effects.
3. Positive separation is observed.

* Current address: Abitibi-Price Inc., Research Centre, Sheridan Park, Mississauga, Ontario, Canada, L5K 1A9.

† To whom correspondence should be addressed.

Journal of Applied Polymer Science, Vol. 35, 1129–1148 (1988)
 CCC 0021-8995/88/051129-20$04.00

However, when solute–membrane affinity dominates:

1. Increasing the operating pressure tends to decrease separation.
2. The permeate flux is significantly less than the pure water flux, even when osmotic pressure effects are negligible (flux reduction).
3. Separation may be positive, negative, or zero, depending on the specific operating conditions.

The study of reverse osmosis in the presence of strong solute–membrane affinity is important. Many current and potential applications of RO, in the food and drug, and petrochemical industries, involve the separation of organics that exhibit this type of behavior. By modelling these types of RO systems a better understanding of membrane separation processes can be achieved.

Temperature is known to be an important operating parameter for reverse osmosis processes, though little is understood as to what role temperature plays in the transport mechanism. Some of the earliest research on temperature effects was done by Lonsdale et al.[8] They performed temperature studies with a sodium chloride–water–cellulose acetate system, and found that permeate flux increased with temperature according to an apparent activation energy of 17.6×10^3 kJ/kmol as described by an Arrhenius equation. The separation did not change with an increase in temperature. From the Stokes-Einstein equation the apparent activation energy for "free" diffusion is 16.7×10^3 kJ/kmol. Therefore an apparent activation energy greater than 16.7×10^3 kJ/kmol implies diffusion through the membrane is "hindered." A hindered diffusion process could be the consequence of molecular steric effects, interaction between solute, solvent, and membrane, and/or some form of flow obstruction. Although the effect of temperature on the performance of reverse osmosis systems is well documented in the literature, especially for the NaCl–water system, little, if any, has been reported on reverse osmosis systems involving strong solute–membrane affinity.

This paper deals with the toluene-water-cellulose acetate reverse osmosis system. The solute, toluene, is known to exhibit strong attraction to cellulose acetate membranes.[4,7,9] The operating variables examined are: applied pressure, feed concentration, and temperature. The main objectives of this research are to: (1) analyze the ability of the finely porous model to describe the experimental data, (2) use the model to describe flux reduction phenomena, (3) observe the effects of temperature on the performance of the system, and (4) modify the finely porous model to account for temperature effects.

THEORY

Several transport relationships are available for the modelling of reverse osmosis transport. Most of the models, however, are inappropriate for reverse osmosis in the presence of strong solute–membrane affinity. A critical review of transport models can be found in the literature.[3,7,10,13] The finely porous transport model however, has been successful in modelling solute systems of this type and is used in this study.

Finely Porous Model. Merten developed the finely porous model based on a balance of applied and frictional forces in a one-dimensional pore. A

complete derivation of the model has been given by Jonsson and Boeson[13] and by Soltanieh and Gill.[10] The model is represented by:

$$1/(1 - f') = b/K_2 + (K_3/K_2 - b/K_2)\exp\{-(X_{AB}/\mathrm{RT})(\tau/\epsilon)N_T/C\} \quad (1)$$

$$N_T = (HC/\tau)/(1 + HC(X_{AM}/\epsilon)\mathrm{X}_{A3})(\Delta P - \Delta\pi) \quad (2)$$

Equation (1) represents the relationship between the separation, f', and the molar flux, N_T. Equation (2) represents the relationship between the effective pressure ($\Delta P - \Delta\pi$), the mole fraction of solute in permeate, X_{A3}, and the total molar flux, N_T. See Nomenclature for complete definitions.

The hydraulic permeability, H, is related to the average pore radius, R_W, by:

$$H = \epsilon R_W^2/8\eta \quad (3)$$

The friction coefficients, X_{AM} and X_{AB}, represent the diffusional friction between the solute and the solvent and between the solute and the membrane, respectively. The relationship between X_{AB} and diffusivity, D_{AB} is:

$$X_{AB} = \mathrm{RT}/D_{AB} \quad (4)$$

The friction parameter, b, is defined[13] as:

$$b = 1 + (X_{AM}/X_{AB}) = D_{AB}/D_{AM} \quad (5)$$

where b represents the friction between solute and membrane relative to the friction between solute and solvent. If X_{AM} equals zero (i.e., insignificant friction forces between solute and membrane) then b is unity and the solvent will pass through the pore by free, unhindered, diffusion. As X_{AM} increases, the value of b increases accordingly, causing a more hindered mode of diffusion.

The separation, based on boundary layer concentration, f' is defined as:

$$f' = (\mathrm{X}_{A2} - \mathrm{X}_{A3})/\mathrm{X}_{A2} \quad (6)$$

The solute concentration at the boundary layer, X_{A2}, is estimated from the "film theory" for membrane separation[14b] as:

$$\mathrm{X}_{A2} = \mathrm{X}_{A3} + (\mathrm{X}_{A1} - \mathrm{X}_{A3})\exp(N_T/kC) \quad (7)$$

Flux Reduction Relationship. Flux reduction is due to strong solute–membrane interaction. The strength of these interactions depends on the affinity and on the effective distance separating the interacting components. Frictional effects are expected to increase as solute–membrane affinity increases, although the exact relationship is not known. Several models have been proposed to describe the effect of strong solute–membrane affinity on flux; two of which are, an empirical approach suggested by Dickson and Lloyd,[4] and a solute sorption approach suggested by Thiel et al.[9] Babai-Pirouz et al.,[15] however, developed a model based on the total flux equation of the

FPM relation. By taking the ratio of pure water flux to solution flux, represented by Eq. (2), and assuming the osmotic pressure, $\Delta\pi$, to be insignificant, this flux reduction relationship is written as:

$$N_P/N_T - 1 = BX_{A3} \tag{8}$$

where B is a parameter relating, $N_P/N_T - 1$ to the permeate concentration, X_{A3}, and is defined as:

$$B = (C/8\eta)R_W^2 X_{AM} \tag{9}$$

Babai-Pirouz used the B relation to describe the flux reduction trends of three cyclic hydrocarbon solutes: 1,3-cyclohexadiene, cyclohexene, and cyclohexane. The B parameter increased with an increase in the nonpolar character of the solute, in the order 1,3 cyclohexadiene < cyclohexene < cyclohexane, and decreased with an increase in the effective pore size of the membrane. Although the data collected were somewhat scattered, the B relation did a reasonable job of representing the data.

Temperature Effects on Membrane Performance. A change in any physical parameter caused by a change in temperature can be modelled by an Arrhenius type function (normalized about reference temperature T°) of the form:[16]

$$U = U°\exp\{(-E/RT°)(\Delta T/T)\} \tag{10}$$

Here, E represents the apparent activation energy of variable U. E is termed the apparent activation energy in order to avoid any confusion with a kinetic activation energy. The Arrhenius equation models the change in a parameter with a change in temperature, but does not imply that an initial energy input is required to activate a change in the parameter.

Chen et al.[16] used the Arrhenius equation to model the change in the permeability coefficient for water and salt solutions at temperatures ranging from 10 to 40°C. Chen found the apparent activation energy to be nearly equal for both types of solution, ranging in value from 15.06×10^3 to 28.87×10^3 kJ/kmol, depending on the membrane studied. Chen also used the Arrhenius equation to interpret the change in experimentally measured partition coefficients, for 0.2M KCl, at various temperatures. The apparent activation energy for the partition coefficient was 17.99×10^3 kJ/kmol.

EXPERIMENTAL

The membrane used in this study was cast according to the Loeb-Sourirajan technique for the fabrication of asymmetric cellulose acetate membranes.[14a] The casting solution was composed of 17.0 wt% cellulose acetate, 69.2 wt% acetone, 12.35 wt% water, and 1.45 wt% magnesium perchlorate. The solution was cooled to 0°C and cast on a glass plate at room temperature with the thickness controlled by a Gardner knife. After a 1 minute evaporation period the membrane was immersed in an ice bath to induce gelling. After one hour the membrane was removed from the glass plate and cut to the appropriate size to be mounted in the flow cell. Prior to

APPARATUS

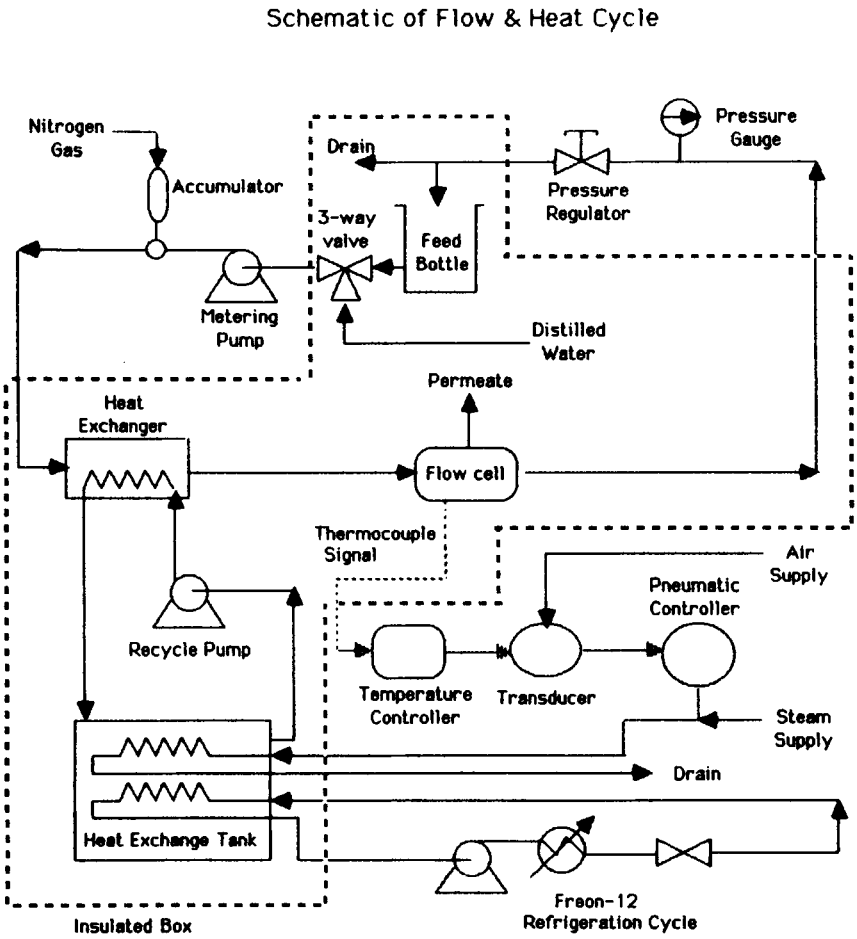

Fig. 1. Schematic of the reverse osmosis test loop with automatic temperature control.

mounting, the membrane was heat treated in an 81°C waterbath for 12 minutes. This annealing step reduces the size of the membrane pores and increases the sodium chloride–water separation. After mounting, the membrane was prepressurized for 8 h at 12,000 kPa to reduce the effect of compaction on subsequent experiments at lower pressures.

The reverse osmosis test system is similar to that reported previously.[7] Briefly, the apparatus consists of a feed reservoir, a high pressure diaphragm metering pump, an accumulator, a radial flow test cell, a pressure gauge, and a back pressure regulator connected in series. An improvement over the previous design is the addition of a temperature control system, as illustrated in Figure 1. The feed solution was heated or cooled by contact with a heat exchange fluid in a shell and tube heat exchanger. The heat exchange fluid (50/50 glycerol and water) was circulated by a centrifugal pump through the

exchanger into a tank containing both a steam heating coil and a freon refrigeration coil. A WEST 2070 microprocessor-based temperature controller measured the temperature in the flow cell and controlled the temperature by regulating the flow of steam to the heating coil. The refrigeration system was closed loop, and was run continuously. The temperature in the flow cell was thus maintained at ± 0.2°C over the operating range of 5 to 35°C.

Sodium chloride experiments (at 10,000 ppm and 7000 kPa) were repeated periodically to characterize the membrane and flow cell, and to monitor any change in membrane behavior over the period of study. For the toluene studies, the feed concentration ranged from 30 to 300 ppm, the operating pressure ranged from 1000 to 7000 kPa, and the operating temperature ranged from 5 to 35°C. The feed flow rate was held constant at 600 mL/min. Sodium chloride concentrations were measured using a YSI Conductivity Bridge (Model 31). The toluene concentrations were measured using a Hewlett Packard Gas Chromatograph (Model 5890). The injected sample was carried by nitrogen gas through a 1.22 m long, 2 mm ID glass column, packed with Porapak "P" (80/100 mesh).

RESULTS AND DISCUSSION

Cell and Membrane Characterization. The pure water and sodium chloride–water experiments were repeated frequently to measure any changes in system performance. The results of these characterization experiments are summarized in Table I. The values listed represent an average of 7 independent experiments repeated at regular intervals during the toluene–water–cellulose acetate membrane system study. The pertinent data include: membrane annealing temperature, pure water mass flux, solution mass flux, pure water permeability coefficient, NaCl–water separation (based on both bulk solution concentration, f, and boundary layer concentration, f'), and mass transfer coefficient.

TABLE I
Characterization and Performance of Cellulose Acetate Membrane in the Radial Flow Cell[a]

Annealing temperature, T, °C	81.0
Pure water molar flux, NP, kmol/m^{2}s $\times 10^4$	5.885 ± 0.003
Solution molar flux, N_T, kmol/m^2 s $\times 10^4$	4.641 ± 0.002
NaCl-Water Separation,	
f, %	91.38 ± 0.50
f', %	95.56 ± 0.48
Pure water permeability coefficient, A, kmol/m^2 s kPa $\times 10^8$	8.3950 ± 0.4352
Mass transfer coefficient, k, m/s $\times 10^5$	1.2140 ± 0.1956

[a] Film area, 1.508×10^{-3} m^2; operating pressure, 7000 kPa; feed concentration, 10,000 ppm NaCl; temperature, 25°C; feed flow rate 600 mL/min. The experimental results are an average of 7 tests, and the error is based on 95% confidence intervals.

The pure water permeability coefficient, A, decreased by 12% over the entire range of experiments. The decrease in A is attributed to membrane compaction. The rate of membrane compaction was notably higher during toluene experiments than for earlier work with just the sodium chloride system. This increased rate of compaction is speculated to be a result of polymer swelling in the presence of organic solute. The swelling of the polymer leads to an increased rate of creep within the membrane structure, which then weakens the compaction resistance of the membrane. Polymer swelling is normally attributed to higher concentrations of organic solute, but the higher interfacial concentration due to polarization effects, and the repeated exposure of organic solute, could ultimately break down the microstructure of the membrane.[7] Although membrane compaction was noted, the separation remained constant (narrow confidence interval) which suggests that the compaction effect did not appreciably alter the average pore size.

Mass Transfer Coefficient. The mass transfer coefficient is largely a characteristic of the flow cell design. The radial flow design was developed as a modification of the flow cell design reported in the literature.[14a] The mass transfer coefficient was determined for NaCl solution at different temperatures using Eq. (7). The value of X_{A2}, needed in Eq. (7), is obtained in the following manner. In Eq. (2), X_{A3} and X_{AM} are small so that $HC(X_{AM}/\epsilon)X_{A3} \ll 1$ for the NaCl–H_2O system and the decrease in flux, compared to pure water flux, is attributed to osmotic pressure effects. Knowing the relationship[14c] between π_i and X_{Ai} gives X_{A2}. The value of k for the NaCl–H_2O system at 25°C is listed in Table I.

Previously, it has been shown that k could be well predicted by a generalized mass transfer correlation of the form:

$$\ln(\mathrm{Sh}/\mathrm{Sc}^{1/3}) \alpha \ln(\mathrm{Re}) \tag{11}$$

where Sh, Sc, and Re are the Sherwood, Schmidt, and Reynolds numbers, respectively. From this equation, k for any solute and temperature can be predicted based on the reference k_{ref} already determined for NaCl–H_2O solution.

$$k = k_{\mathrm{ref}}(D_{AB}/D_{AB,\mathrm{ref}})^{0.66}(\nu/\nu_{\mathrm{ref}})^{0.04} \tag{12}$$

The above equation was tested by measuring k at different temperatures and comparing to the predicted value. Good agreement was found as illustrated in Figure 2. Equation (12) was used to predict the value of k for the toluene–water–cellulose acetate system, at various temperatures, using the known value of k for the sodium chloride–water–cellulose system at 25°C. The values of D_{AB} for toluene at different temperatures were estimated by the Wilke–Chang equation.[17] The predictions of k for both sodium chloride and toluene solutes are shown in Table II.

Flux versus Separation. The finely porous model (FPM) was fit to the experimental data for the separation of toluene and water under various operating conditions. The parameters of the FPM relationship were estimated by a nonlinear regression analysis. The parameters were grouped as: $\beta_1 = b/K_2$, $\beta_2 = (K_3/K_2 - b/K_2)$, and $\beta_3 = (X_{AB}/\mathrm{RT})(\tau/\epsilon)$. The form of the equation for data analysis was:

$$f' = [(\beta_1 - 1) + \beta_2 \exp(\beta_3 N_T/C)]/[\beta_1 + \beta_2 \exp(\beta_3 N_T/C)] \tag{13}$$

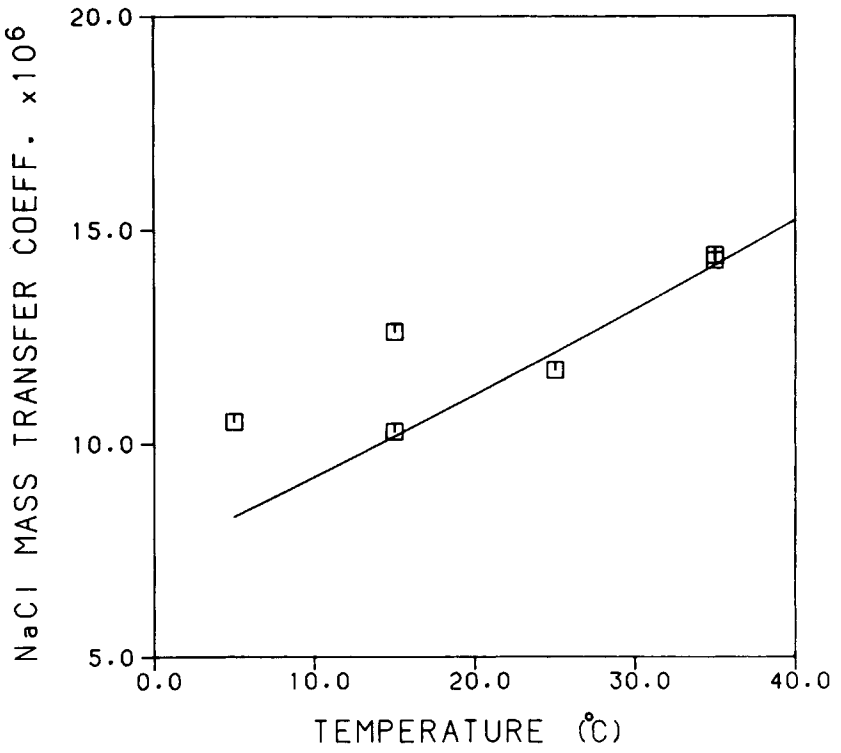

Fig. 2. The effect of temperature on the mass transfer coefficient for NaCl. (□) experimental data, (—) generalized mass transfer correlation.

TABLE II
Predicted Mass Transfer Coefficients at Various Temperatures

Temperature °C	Mass Transfer Coefficient m/s, × 10^6	
	k_{NaCl}	$k_{C_7H_8}$
5	8.583	5.962
15	9.891	6.871
25	11.80	8.195
35	13.82	9.595

The computer program acted to find the values of β_1, β_2, and β_3 that minimized the sum of the squares error between experimental and model f' values.

The results of the FPM relationship fitting are summarized in Table III and in Figures 3–5. The agreement between model and data is good. The standard deviation, s, is small, signifying an accurate fit. The model does an excellent job of following the data trend of decreasing separation with increasing flux; a behavior that most transport models cannot account for.

The first model parameter b/K_2 (Table III) is greater than unity for both 5 and 25°C, and decreases slightly with an increase in temperature. The second model parameter, $K_3/K_2 - b/K_2$, increases significantly with an increase in

TABLE III
FPM Parameters

	5°C	25°C	35°C
β_1 (b/K_2)	1.6647	1.3706	444.42
β_2 $(K_3/K_2 - b/K_2)$	0.1706	0.7065	442.44
$\beta_3, \times 10^{-5}$ $(X_{AB}/\mathrm{RT})(\tau/\epsilon)$	6.2744	1.4444	2.1345×10^{-3}
Standard deviation (s)	0.0268	0.0164	0.0613

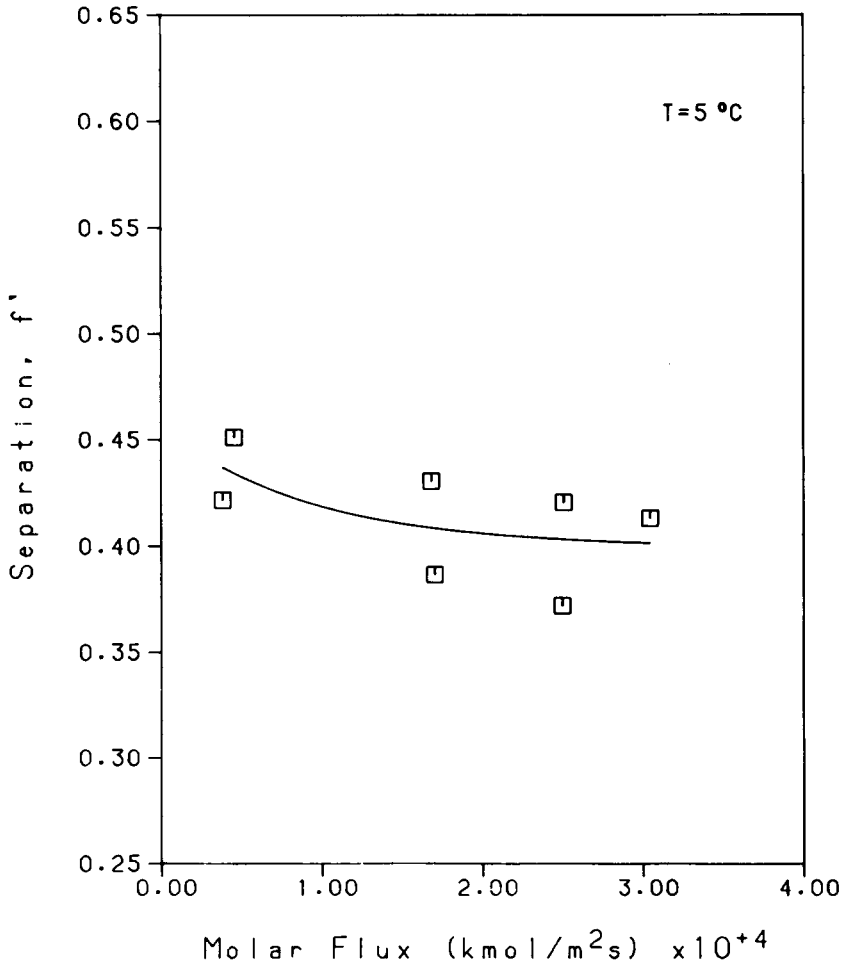

Fig. 3. The correlation of separation, f', and the molar flux, N_T, for toluene–water–cellulose acetate membrane system at 5°C. (□) experimental data, (—) finely porous model.

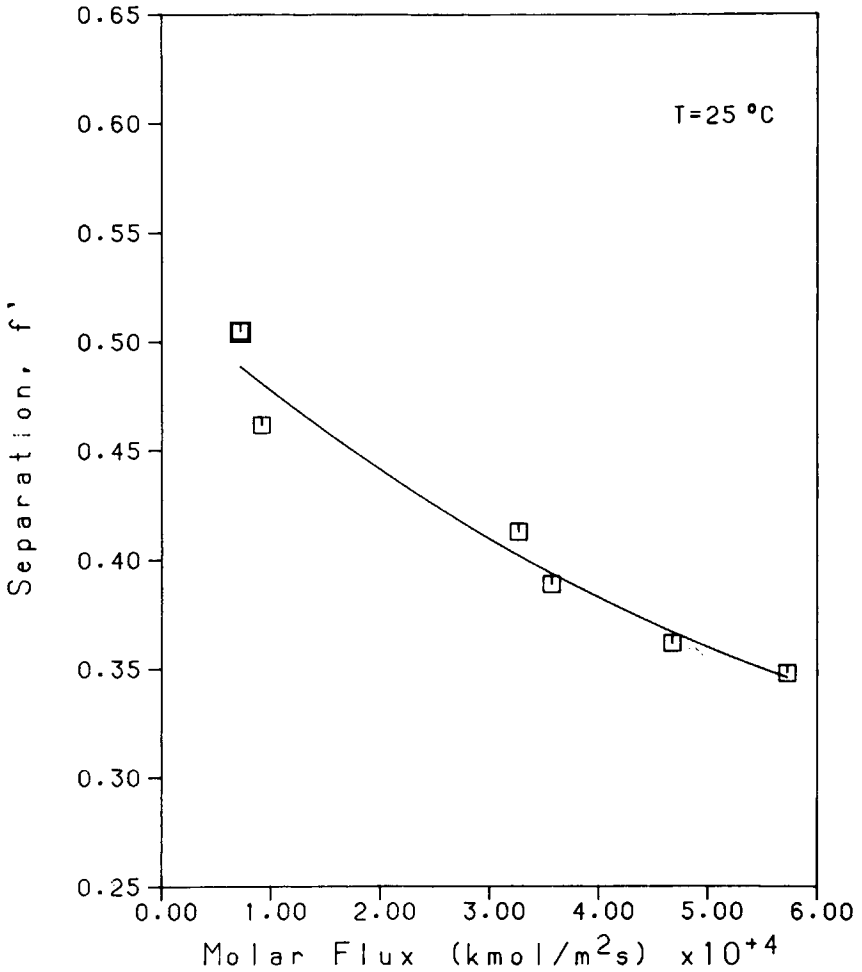

Fig. 4. The correlation of separation, f', and the molar flux, N_T, for toluene–water–cellulose acetate membrane system at 25°C. (□) experimental data, (—) finely porous model.

temperature, while the third model parameter, $(X_{AB}/\mathrm{RT})(\tau/\epsilon)$, showed a marked decrease with an increase in temperature.

The experimental data at 35°C are scattered and do not conform to the trends observed at 5°C and 25°C. The reason for this behavior is not understood; although it is apparent that this effect is unaccounted for by the model prediction. As a result of the anomaly, model predictions at 35°C are excluded from further analysis of the separation behavior.

The behavior of decreasing separation with increasing flux is a unique characteristic of RO in the presence of strong solute–membrane affinity. One possible explanation for this sort of behavior is that as pressure is increased the velocity of permeating fluid also increases resulting in an increase in flux. The increased velocity causes an increase in the mobility of the solute due to an increase in shear effect at the interfacial solute layer. The increased solute mobility results in an increased ratio of solute to solvent flow and thus a decrease in separation performance. The solute–water separation may be positive, negative, or zero depending on the strength of attraction between the

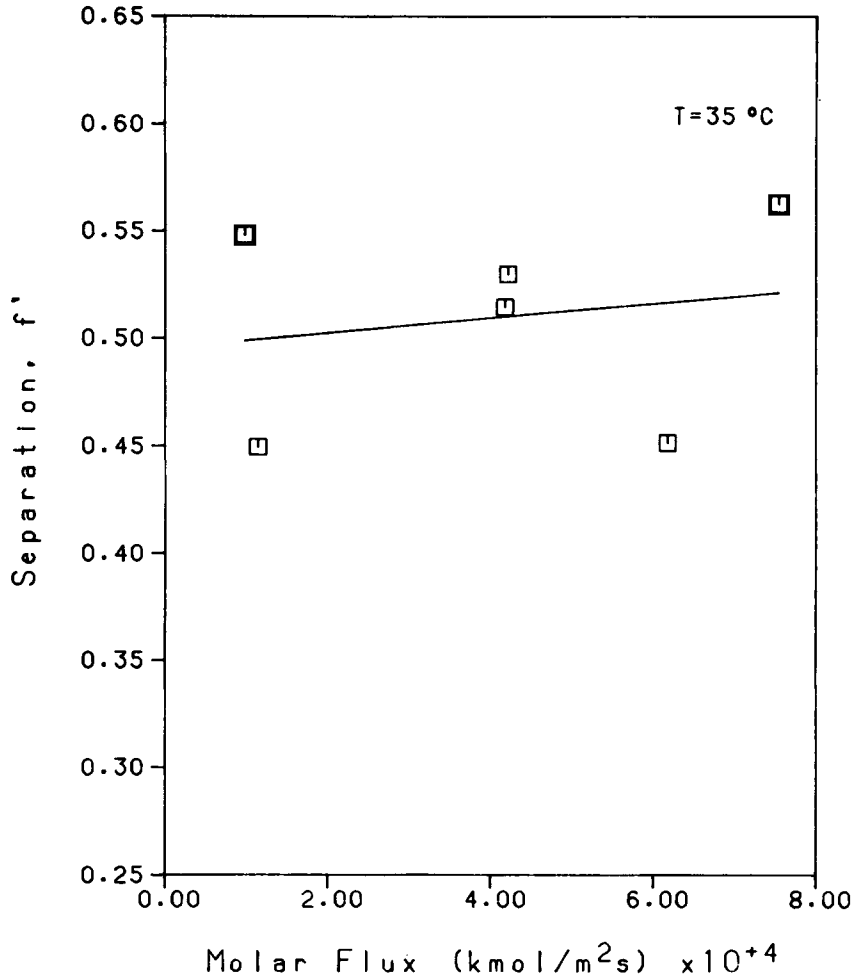

Fig. 5. The correlation of separation, f', and the molar flux, N_T, for toluene–water–cellulose acetate membrane system at 35°C. (□) experimental data, (—) finely porous model.

solute and the membrane, along with specific operating conditions. When these factors are such that the solute-membrane interactions are relatively weak, the solute solution in the interfacial region is carried through the pore with relatively little resistance, resulting in negative separation. When these factors are such that the solute–membrane attraction is relatively strong, the solute in the interfacial region is immobilized at the membrane surface, resulting in positive separation. When these factors are balanced, the solute concentration remains unchanged from the high to low pressure sides of the membrane and the separation is zero. The data for toluene-water indicated positive separation, thus the attraction between solute and membrane is relatively strong for a toluene–cellulose acetate system. Similar behavior has been reported in the literature.[7,18]

Flux Reduction Relationship. Flux reduction is usually observed for systems involving strong solute–membrane attraction. The strength of attraction depends on the affinity between the interacting components and the effective distance separating the components. According to the FPM relation-

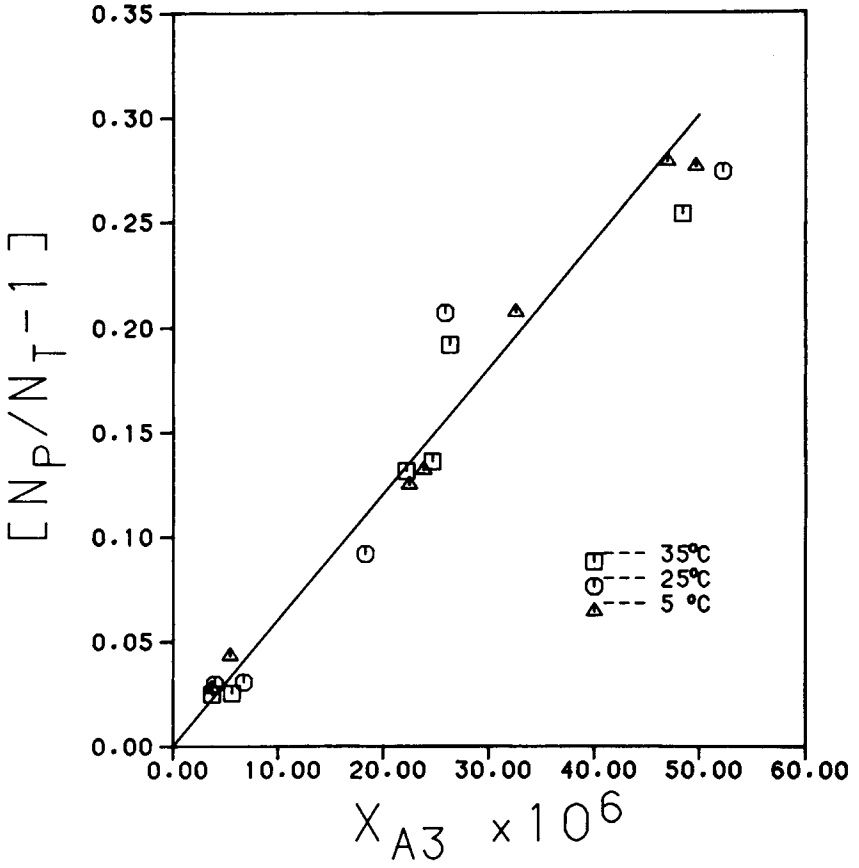

Fig. 6. Flux reduction relationship for the system toluene–water–cellulose acetate membrane at three different temperatures. (Δ, ○, □) experimental data, (—) finely porous model.

ship the flux reduction is attributed to a strong frictional force acting between the solute and the membrane, which acts to reduce the velocity of the pore fluid. As derived previously, the relationship between flux and permeate concentrations for dilute solutions is given by Eqs. (8) and (9).

The experimental data at 5, 25, and 35°C are plotted, in the form suggested by Eq. (8), in Figure 6. A clear agreement is found between the model and the data at all three temperatures. The slope, B, was calculated and compared for the three temperatures. The 95% confidence intervals on B overlapped; therefore it was concluded that B was independent of the temperature for the range studied. The pooled average value of B is 6021.

Parameter Interpretation. In order to analyze the validity of the physical parameters represented by the FPM relationship, it is necessary to quantify the components within the model. In the previous section the parameters, B, β_1, β_2, and β_3 were determined. These values can be used to determine most of the physical parameters in the model. τ/ϵ is known directly from β_3 and Eq. (4). Rearranging Eq. (9) and substituting into Eq. (3) leads to:

$$X_{AM} = B/[(HC/\tau)(\tau/\epsilon)] \tag{14}$$

TABLE IV
FPM Parameters

	5°C	25°C
Model		
b	129.1	121.6
τ/ϵ (m)	3.044×10^{-4}	1.250×10^{-4}
R_W (m)	1.478×10^{-9}	1.499×10^{-9}
K_2	77.54	88.73
K_3	142.3	184.3
X_{AM} (m s kPa/kmol)	6.060×10^{14}	3.341×10^{14}
Theoretical		
$X_{AM,\text{Faxen}}$ (m s kPa/kmol)	2.775×10^{12}	1.739×10^{12}
X_{AB} (m s kPa/kmol)	4.695×10^{12}	2.770×10^{12}

where $A = HC/\tau$. Therefore all the quantities in Eq. (14) are known and X_{AM} can be calculated. Multiplying both sides of Eq. (3) by C/τ and rearranging gives:

$$A = HC/\tau = R_W^2 C/(8\eta(\tau/\epsilon)) \tag{15}$$

Therefore, the average pore size, R_W, can be calculated. Combining known values of X_{AB}, X_{AM}, and Eq. (5) gives b. Substituting b into the definition of β_1 and β_2, the partition coefficients K_2 and K_3 are calculated. Therefore, from the above calculations, all of the physical parameters in the model have been separated into component parts except τ/ϵ. Without some independent measure of the pore length or pore area, τ and ϵ cannot be determined explicitly. The values of the parameters are summarized in Table IV.

The experimental value of X_{AM} can be compared to the theoretical value of X_{AM} calculated from the Faxen equation. The Faxen equation describes the friction drag exerted on a sphere as it passes through the center line of a narrow cylinder.[19] If this equation is adapted to a membrane transport system, the analytical solution is:

$$1/b_{\text{Faxen}} = 1 - 2.104\lambda + 2.09\lambda^3 - 0.95\lambda^5 \tag{16}$$

where b_{Faxen} is the friction parameter and λ is the ratio of solute molecular radius to the membrane pore radius, R_A/R_W. The radius of the solute is estimated from the Stokes–Einstein equation to be 2.830×10^{-10} m, at 25°C. From Eq. (5) and Eq. (16) the theoretical value of $X_{AM,\text{Faxen}}$ can be determined.

X_{AM} represents the force of friction between the solute and the membrane. Compared to the theoretical value, $X_{AM,\text{Faxen}}$, the experimental value, X_{AM}, is two orders of magnitude larger. This discrepancy is large. It is apparent that X_{AM} from the FPM relationship contains a resistance force unaccounted for by the Faxen equation. It is reasonable to assume that the discrepancy

between the theoretical and experimental values of X_{AM} is due to physicochemical attraction between solute and membrane. As well, X_{AM} is two orders of magnitude larger than X_{AB}, which reflects the decreased mobility of the solute in the pore compared to the solute in free solution. Previously, others have also found that the Faxen equation would underestimate the drag when the solute was attracted to the membrane.[20]

The temperature dependence of X_{AM} can be understood by examining the temperature dependence of X_{AB}. By Eq. (4), X_{AB} is proportional to T/D_{AB} and from the Wilke–Chang equation[17] D_{AB} is proportional to T/η. Therefore, X_{AB} decreases with an increase in temperature according to the apparent activation energy of viscosity; from 5 to 35°C, X_{AB} decreases by 41%. This compares favorably with the observed 45% decrease in X_{AM} over the same temperature change. As a first approximation, the temperature dependence of X_{AM} is determined by the change in the viscosity of the solution.

The value of b is a function of X_{AM} and X_{AB} given by Eq. (5). According to the above discussion, b should be independent of temperature, since X_{AM} and X_{AB} have the same apparent activation energy. Table IV illustrates that b remains relatively constant. Similarly, B, given by Eq. (9), is dependent on X_{AM}/η so that the temperature effects cancel out. Therefore, it is not surprising that B was found to be temperature independent.

The τ/ϵ parameter represents the effective pore length divided by the membrane pore area. The decreased value of τ/ϵ with an increase in temperature is assumed to be a result of experimental error. Since experiments are conducted well below the glass transition temperature of cellulose acetate ($\simeq$ 65°C), the membrane pore diameter and pore distribution are assumed to be insensitive to temperature effects. The average value of τ/ϵ is 2.147×10^{-4} m, which compares favorably to data presented previously.[7] It was expected that R_W should also be independent of temperature. Therefore, R_W was calculated based on the average value for τ/ϵ. An average value of $R_W = 1.489 \times 10^{-9}$ m was used in the remaining calculations. This pore size is reasonable for the cellulose acetate membrane used.[7]

K_2^* and K_3 represent the partition coefficients on the high and low pressure sides of the membrane, respectively. The K_3 value is about twice the size of K_2 value, which clearly indicates that the partition coefficient is not constant. The partition coefficient most likely changes because of a dependence on concentration or a dependence on membrane structure. The ratio of K_3/K_2 is average to be 1.96, which is comparable to data presented earlier.[7] Both K_2 and K_3 increase with an increase in temperature according to activation energies of 10.50×10^3 and 14.85×10^3 kJ/kmol, respectively. Chen et al.[16] also found the partition coefficient to increase with temperature. Chen measured the partition coefficient for a 0.2M KCl solution over a range of temperatures from 10 to 40°C, and estimated an apparent activation energy of 17.99×10^3 kJ/kmol. This value of E is of the same magnitude as that for the toluene–water–cellulose acetate system, suggesting that the parameter estimations and representations of the FPM relation are valid.

In overview, the FPM relationship does a good job of representing the data trends exhibited by the toluene–water–cellulose acetate system. The use of temperature as an operating variable supplies an additional avenue for evaluating model accuracy and analyzing parameter values. The physical

TABLE V
FPM Parameter Apparent Activation Energies

Parameter	Parameter activation energy E, kJ/kmol, $\times 10^{-3}$
$\beta_1 = b/K_2$	−6.70
$\beta_2 = (K_3/K_2 - b/K_2)$	30.38
$\beta_3 = (X_{AB}/\mathrm{RT})(\tau/\epsilon)$	−50.64

representation of parameters within the FPM relationship appear to follow the expected temperature dependencies of the parameters they represent.

Further study with the FPM relationship is needed before firm conclusions about the mechanism of RO can be stated. In this work, for the first time, it has been demonstrated how the individual values of R_W, b, X_{AM}, K_2, and K_3 can be estimated based on permeation data only. Once these parameters are known, it is relatively easy to compare physical model parameters with independently estimated counterparts. It is suggested that a more rigorous experimental study be conducted on a variety of solutes over a wide range of pressures, concentrations, and temperatures. It is also important to independently measure the partition coefficients for these solutes. By comparing the measured partition coefficient with those found from FPM relationship, quantitative statements can be made about the accuracy and the validity of the physical parameter representation defined by the finely porous model.

Modelling of Temperature Effects

The Arrenhius expression is used to interpret the change in finely porous transport parameters with temperature. The apparent activation energy of β_1, β_2, and β_3 are calculated directly from model-fitting information in Table III. The apparent activation energies for the parameters are presented in Table V.

The apparent activation for β_4 is estimated from prior information. Combining Eqs. (2) and (9), the molar flux, N_T, can be expressed as:

$$N_T = [A/(1 + BX_{A3})](\Delta P - \Delta\pi) \tag{17}$$

For dilute solutions $\Delta\pi$ can be assumed zero. From flux reduction data, B is known to be 6021 and is temperature independent. The average value of the pure water permeability coefficient, A, at 25°C is 8.395×10^{-8} kmol/m^2 s kPa, from Table I. Pure water experiments during hydrocarbon testing indicate that A changes with temperature according to an apparent activation energy of 22.01×10^3 kJ/kmol. This dependency is illustrated in Figure 7. Note that this value of the apparent activation energy is slightly higher than that given for earlier water experiments. Two possible sources for this discrepancy are: mild compaction effects causing diffusion hindrance, or experimental error.

When the apparent activation energy for each model parameter is substituted into the FPM relationship, an expression for RO transport is formed

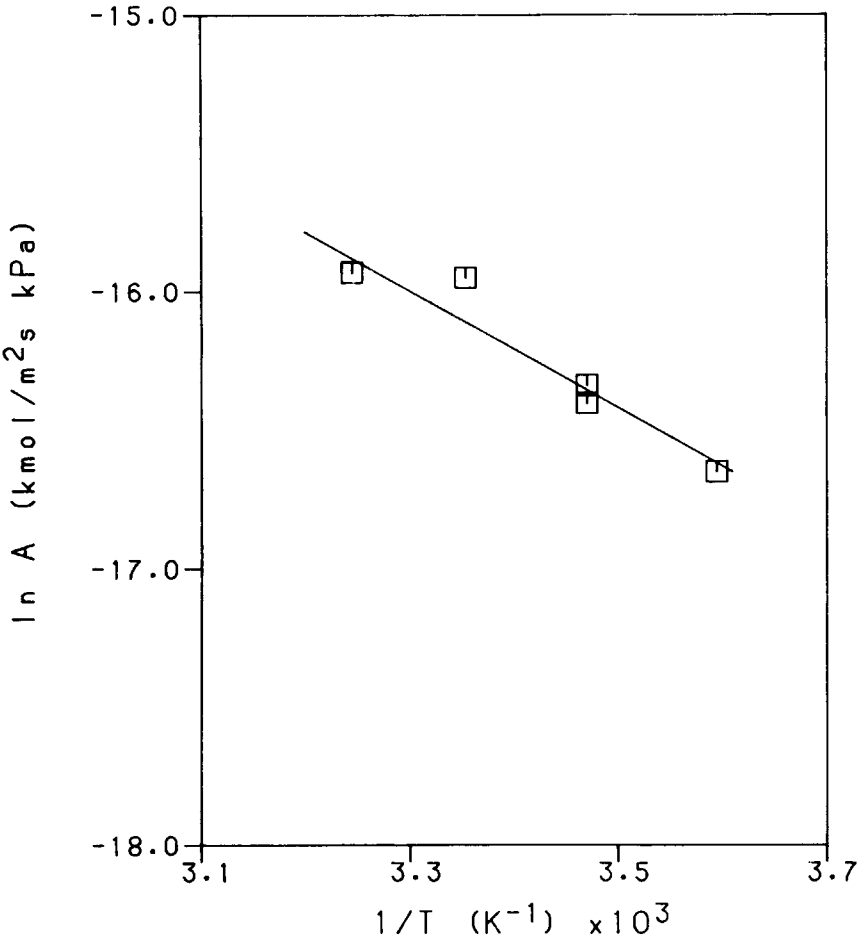

Fig. 7. Arrhenius type plot for the pure water permeability coefficient as a function of temperature for the cellulose acetate membrane. (□) experimental data, (—) Arrhenius equation.

that accounts for changes in temperature. The new model is written as:

$$1/(1-f') = X_{A2}/X_{A3}$$
$$= \beta_1 \exp\{-(-6.70 \times 10^{+3}/RT°)(\Delta T/T)\}$$
$$+ \beta_2 \exp\{-(30.38 \times 10^{+3}/RT°)(\Delta T/T)\}$$
$$\times \exp[-\beta_3 \exp\{-(-50.64 \times 10^{+3}/RT°)(\Delta T/T)\} N_T/C] \quad (18)$$

where

$$\beta_1 = b/K_2$$
$$\beta_2 = (K_3/K_2 - b/K_2)$$
$$\beta_3 = X_{AB}(\tau/\epsilon)/RT$$

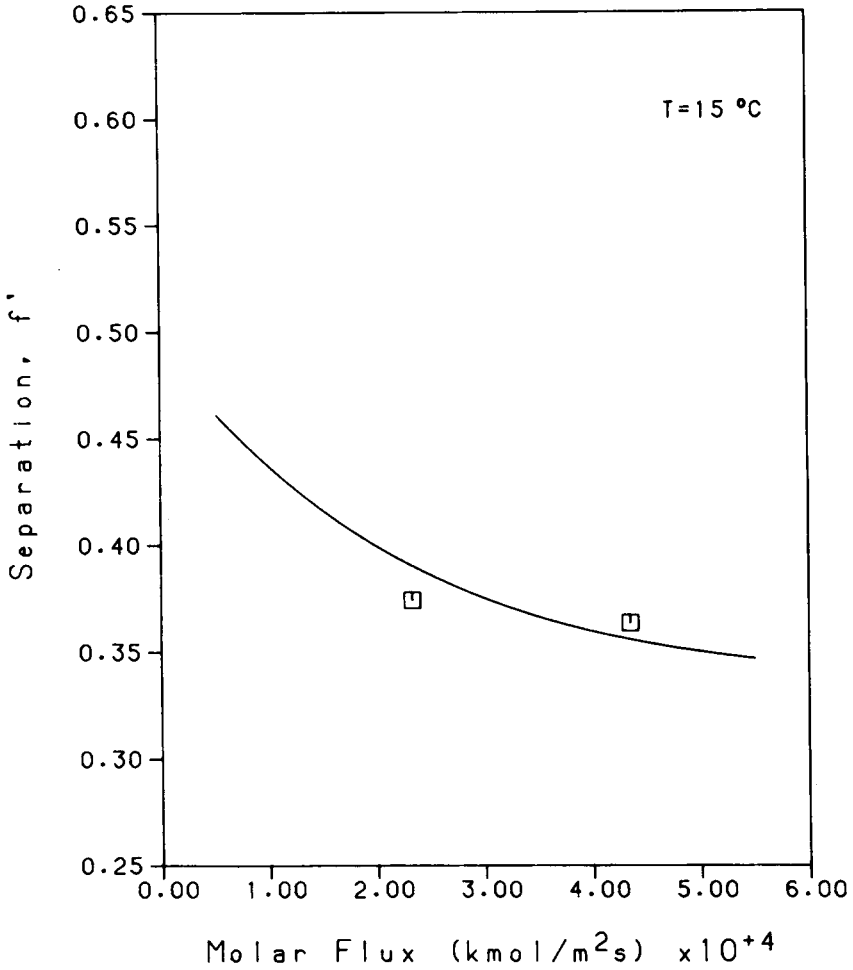

Fig. 8. Prediction of the separation and flux at 15°C based on the finely porous model. (□) experimental data, (—) predication.

and $T^\circ = 298.15$ K

$$N_T = \beta_4(\Delta P - \Delta\pi) \tag{19}$$

where

$$\beta_4 = A \exp\{-(22.01 \times 10^{+3}/RT^\circ)(\Delta T/T)\}/(1 + BX_{A3})$$

and $T^\circ = 298.15$ K

For a given operating pressure, feed concentration, and temperature, the value of X_{A3} and N_T can be predicted by simultaneously solving Eqs. (18) and (19). The predicted relationship between separation and flux at 15°C is illustrated in Figure 8. The two data points in Figure 8 represent toluene–water–cellulose acetate system experiments conducted at 15°C. As can be seen, the generated curve for operation at 15°C does an excellent job of predicting the actual separation versus flux data.

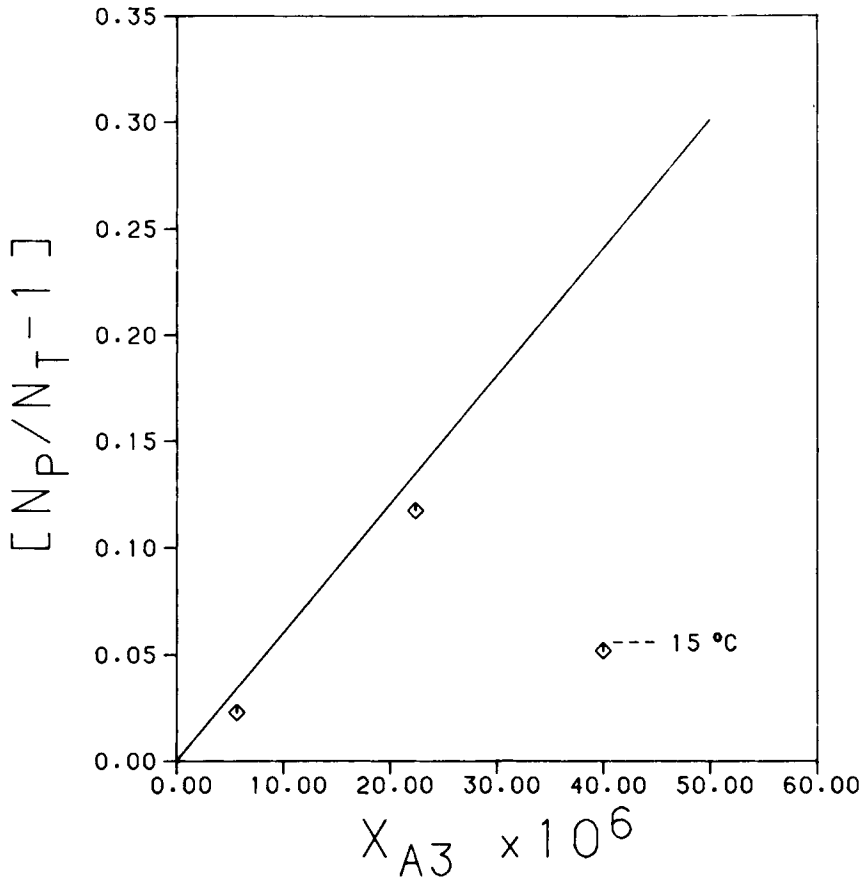

Fig. 9. Prediction of the flux reduction at 15°C based on the finely porous model. (□) experimental data, (—) predication.

Figure 9 illustrates the B relationship using the pooled average value of B from Table V. The data points in Figure 9 represent flux reduction, as calculated from the B relation, for experiments conducted at 15°C. As can be seen, the pooled average value for the B relation does a good job of predicting the flux reduction versus solute concentration at 15°C.

CONCLUSIONS

Experimental data were collected for the toluene–water–cellulose acetate membrane system at different pressures in the range 1000–7000 kPa, at different concentrations in the range of 30–300 ppm toluene, and at different temperatures in the range 5–35°C. The mass transfer coefficient for the test cell was calculated based on sodium chloride data at different temperatures. A generalized mass transfer correlation was evaluated and found to do a good job of describing the effect of temperature on the mass transfer coefficient.

The finely porous model was used to describe the toluene-water separation and flux data. The agreement between the model and the data was good. The individual parameters in the model were determined and compared to expec-

tations. It was found that the partition coefficient was different on high and low pressure sides of the membrane. The model was extended to include the effects of temperature over a range of variables studied. This model was used to predict the performance of the membrane at 15°C and the agreement with the actual experimental data was excellent.

NOMENCLATURE

A	pure water permeability coefficient, kmol/m^2 s kPa.
b	friction parameter as defined by Eq. (5).
b_{Faxen}	friction parameter as defined by Eq. (16).
B	flux reduction parameter.
C	molar density of solution, kmol/m^3.
D_{ij}	diffusivity of component i in component j, m^2/s.
E	apparent activation energy, kJ/kmol.
f	separation.
f'	separation based on the boundary layer concentration.
h	characteristic cell dimension, m.
H	hydaulic permeability, m^2 s/kPa.
J_V	solvent volume flux, m^3/m^2 s.
K_i	solution partition coefficient at location i.
k	mass transfer coefficient, m/s.
N_i	molar flux of i, kmol/m^2 s.
ΔP	pressure difference across the membrane, kPa.
Q	feed flow rate, m^3/s.
R	gas constant, 8.314 kJ/kmol K.
Re	Reynolds number, $Q/h\nu$.
R_A	effective radius of solute, m.
R_W	radius of a pore, m.
Sc	Schmidt number, ν/D_{AB}.
Sh	Sherwood number, kh/D_{AB}.
s	standard deviation.
T	temperature, K.
T°	normalized temperature, K.
ΔT	defined as T° − T.
U	variable defined in Eq. (10).
$U°$	variable defined in Eq. (10).
X_{Ai}	mole fraction of solute at location i.

Greek Symbols

$\beta_1, \beta_2, \beta_3, \beta_4$	model parameters.
ϵ	fractional pore area.
η	solution viscosity, kPa s.
λ	ratio of solute radius to pore radius.
ν	kinematic viscosity of the solution, m^2/s.
$\Delta\pi$	osmotic pressure difference across the membrane, kPa.
τ	the effective thickness of the membrane, m.
X_{ij}	friction coefficient between component i and j, m s kPa/kmol.

Subscripts

A	solute
B	solvent
M	membrane
P	pure water
ref	reference solute, NaCl
T	total solution
W	wall
1	feed solution
2	boundary layer solution
3	permeate solution

References

1. T. Matsuura, S. Sourirajan, *J. Appl. Polymer Sci.*, **17**, 3683 (1973).
2. T. Matsuura, J. M. Dickson, and S. Sourirajan, *J. Appl. Polymer Sci.*, **15**, 149 (1976).
3. H. G. Burghoff, K. L. Lee, and W. Pusch, *J. Appl. Polymer Sci.*, **25**, 323 (1980).
4. J. M. Dickson and D. R. Lloyd, in *Synthetic Membranes*, A. F. Turbak, Ed.; ACS Symposium Series: Washington, D.C., 1981.
5. J. M. Dickson, M. Babai-Pirouz, and D. R. Lloyd, *Ind. Eng. Chem. Process Des. Dev.*, **22**, 625 (1983).
6. D. R. Lloyd, M. Babai-Pirouz, and J. M. Dickson, *J. Sep. Process Tech.*, **3**, 21 (1982).
7. J. M. Dickson, Ph.D. dissertation, Virginia Polytechnic Institute and State University; Blacksburg, VA, 1985.
8. H. K. Londsdale, U. Merten, and R. L. Riley, *J. Appl. Polymer Sci.*, **9**, 1341 (1965).
9. S. W. Thiel, D. R. Lloyd, and J. M. Dickson, in *Reverse Osmosis and Ultrafiltration*, S. Sourirajan, Ed.; ACS Symposium Series 281, 1986, Chap. 10.
10. M. Soltanieh, and W. N. Gill, *Chem. Eng. Commun.*, **12**, 279 (1981).
11. G. Jonsson, *Desalination*, **24**, 19 (1978).
12. G. Jonsson, *Desalination*, **35**, 21 (1980).
13. G. Jonsson and C. E. Boeson, *Desalination*, **17**, 145 (1975).
14. S. Sourirajan, *Reverse Osmosis*, Academic Press: New York, 1970; (a) Chapter 2, (b) Chapter 3, (c) Appendix.
15. M. Babai-Pirouz, S. W. Thiel, D. R. Lloyd, and J. M. Dickson, *J. Membr. Sci.*, **21**, 21 (1984).
16. Y. Chen, H. Nomura, and W. Pusch, *Desalination*, **46**, 437 (1983).
17. C. R. Wilke and P. Chang, *AIChE J.*, **1**, 264 (1955).
18. T. Matsuura and S. Sourirajan, *Ind. Eng. Chem. Process Des. Dev.*, **5**, 33 (1978).
19. H. Faxen, *Arkiv. Mat. Astron. Fys.*, **17**, No. 27 (1923).
20. C. N. Satterfield, C. K. Colton, and W. H. Pitcher Jr., *AIChE J.*, **19**, 628 (1973).

Received January 8, 1987
Accepted February 3, 1987